Filament Recycling and Sustained Contractile Flows in an Actomyosin Cortex

William McFadden[1], Jonathan Michaux[2], Patrick McCall[3], Edwin Munro[2,*]

1 Biophysical Sciences Program, University of Chicago, Chicago, IL, USA
2 Department of Molecular Genetics and Cell Biology, University of Chicago, Chicago, IL, USA
3 Department of Physics, University of Chicago, Chicago, IL, USA

*** emunro@uchicago.edu**

Abstract

Fill in abstract later.

Author Summary

In this paper, we develop and analyze a minimal model for 2D active networks based on the cortical cytoskeleton of eukaryotic embryos. Our model introduces a drag-like slip between cross-linked filaments as means to dissipate stored stress, generating a macroscopic effective viscosity. We further introduce an active friction to active stress from microscopic properties. We generate computational simulations based on the model, and demonstrate that active stress is sufficient to drive network contraction only temporarily. By introducing filament recycling, we are able to set up steady state flow profiles such as those found in the cortex of developing embryos and migrating cells. The model is used to calculate phenomenological constants measured in prior experiments. Our analysis sheds insight on potential microscopic control parameters governing broad qualitative differences in 2D active networks. We make our model freely accessible and our methodology transparent to enable other researchers to clearly understand our modeling framework and to build upon our findings.

Introduction

The ability of animal cells to deform rapidly and irreversibly is essential for many aspects of development and physiology. One of the most striking examples of cellular deformation are flows that arise within the actomyosin cortex, a thin layer of cross-linked actin filaments and myosin motors that lies just beneath the plasma membrane. Cortical flows play key roles in cell polarization, cell division, cell crawling and multicellular tissue morphogenesis [1, 2]. Cortical flows are governed by a dynamical interplay of active local force generation and passive force relaxation. Active forces are thought to be primarily generated by myosin motors pulling against individual actin filaments and these are then transmitted through cross-linked networks to produce macroscopic stress [3], though the details this process is still not well understood. Importantly, the actomyosin cortex is highly dynamic; filaments are disassembled and reassembled continuously, with a typical monomer lifetime of just tens of seconds.

Dynamic filament recycling is essential to allow remodelling of cellular structure during development and physiology, but how this works remains poorly understood as well. Here, we focus on exploring how dynamic cross-links and actin filament recycling can tune rates of network deformation to allow cells to generate steady-state actomyosin flows, which are a crucial element of cell polarization and cell migration.

Cortical flows arise from active motors generating stresses in a viscously relaxing network. Our current understanding of the physics of cortical flows arises from the physics of active fluids [4]. In this model, the pattern of flow arises in response to gradients in internal active stress arising from local imbalances in active motor concentration [5]. These theories have had much success in explaining macroscopic patterns such as the formation of contractile rings [6]. Both active stress and passive relaxation will be highly dependent on a microscopic parameters such as network density and turnover rates, and there has already been a great deal of work done one deriving the microscopic scale understanding of contractile actin networks. However, there is still a gap between how these microscopic parameters relate to local properties and what influence this will have on large-scale macroscopic flows. Our aim is to build a minimal microscopic model of an active, cross-linked filament network with turnover that will allow us to draw direct comparisons to macroscopic levels of stress buildup, stress relaxation, and cortical flow velocity.

At long timescales, cross-linked filament networks relax their internal stresses. Fluid-like stress relaxation have been observed in a number of cellular processes [1, 2, 4, 7–9]. These modes of stress relaxation are predominantly believed to arise from both the transient binding of cross-links and from the rapid turnover of filaments. In *in vitro* studies, long timescale creep behaviors are thought to arise predominantly from the transient nature of filament binding for most biologically relevant cross-linkers [10–14]. However, the rapid rates of stress relaxation needed to produce large scale cell shape changes have made it clear that rapid actin turnover must play a significant role as well. Indeed, energy consuming biochemical processes drive the rapid disassembly and reassembly of actin filaments, through a process we call filament recycling. Although several theoretical methods have addressed cross-link binding and unbinding analytically [15, 16] and others have explicitly modeled reversible cross-linking in combination with complex mechanics of filament bundles [12, 17, 18], less attention has been paid to actin turnover as mechanism of stress relaxation. However, recent efforts have begun to the fluid like properties of networks under applied stresses [19], and some experimental work is beginning to elucidate their mechanical properties [Cite McCall].

Current understanding of stress generation in disordered active networks The coordinated action of actin and myosin alone has been show to be sufficient to drive contraction in synthetic systems [20]. Filament extensional asymmetry and dispersion in motor activity are sufficient conditions for the contraction in one [21] and two [22] dimensional networks. Further work has explored a multitude of microscopic parameters that can tune contractile patterns [23–25] or mechanical properties of networks [26, 27]. However all of these examples generate momentary contraction which eventually stalls. More recent efforts have begun to elucidate how network turnover can generate sustained flows [28], and several modeling efforts have begun to view how long term stalling can be avoided in the presence of filament turnover [29, 30]. These systems of contractile material with turnover can generate highly dynamic behaviors [31], but much work remains to understand the general principles underlying these results.

Our model allows calculation of results at long-timescales while incorporating a coarse-grained micro-scale model. To incorporate as much micro-scale detail as possible while still maintaining the generality of the active fluid theory, we introduce several coarse-grained approximations into our representation of filament networks. First, we simplify the complex asymmetric compliance of semi-flexible polymers with a simple asymmetric spring compliance. Second, we simplify cross-linking via filament drag-like coupling in which filaments are able to slide past each other as molecular bonds form and rupture, akin to coarse-grained models of molecular friction [32–34]. Third, our networks are imbued with dispersion of activity by making a subset of filament overlaps into "active" cross-links [35]. Finally, we generate filament turnover by regularly reseting a subset of filaments to a new unstrained position. Importantly, these simplification allows us to extend our single polymer models to dynamical systems of larger network models for direct comparison between theory and modeling results. This level of coarse graining will therefore make it easier to understand classes of behavior for varying compositions of cross-linked filament networks. In addition, it allows us to compute a new class of numerical simulations efficiently, which gives us concrete predictions for behaviors in widely different networks with measurable dependencies on molecular details.

We have used our model to investigate how rates of flow will depend on microscopic properties of networks. Another quick summary which will be easy after the paper is written.

Models

We choose to focus our attention on 2D networks both for their tractability as well as their relevance in the quasi-2D cytoskeletal cortex of many eukaryotic cells [4]. In addition, recent developments in 2D *in vitro* systems [20, 36], make 2D disordered models all the more interesting as a renewed focus of study. In the rest of this section, we underline the key points necessary for understanding our modeling framework and the key assumptions we have made in generating our equations of motion for the system.

Asymmetric Filament Compliance

We model individual filaments as chains of springs with relaxed length l_s. Filaments can therefore be represented as a sequence of nodes with positions $\mathbf{x_i}$ and nearest neighbor force interactions, $\mathbf{F_i^\mu}$, of the form

$$|F_i^\mu| = \mu \cdot \frac{|\mathbf{x_{i+1}} - \mathbf{x_i}| - l_s}{l_s} + \mu \cdot \frac{|\mathbf{x_{i-1}} - \mathbf{x_i}| - l_s}{l_s} \tag{1}$$

where, μ represents an extensional modulus of a filament. Here, we take the modulus, μ, to have a different value depending on whether $|\mathbf{x_{i-1}} - \mathbf{x_i}| - l_s$ is greater or less than 0. This moduli is a composite quantity related to both filament and cross-linker compliance in a manner similar to a proposed effective medium theory [37]. In the limit of highly rigid cross-links and flexible filaments, our model reduces to the pure semi-flexible filament models of [38, 39]. In the opposite regime of nearly rigid filaments and highly flexible cross links, our method is still largely similar to the model of [37] in small strain regimes before any nonlinear cross link stiffening. However, in departure from those models, the magnitude of the force on interior cross-links in our model is still the same as those on the exterior. This is a simplification of the varying levels of strain that would actually be present in these cross-linkers as addressed in [37], but we choose to ignore the slight variation in favor of an approximated, global mean approach.

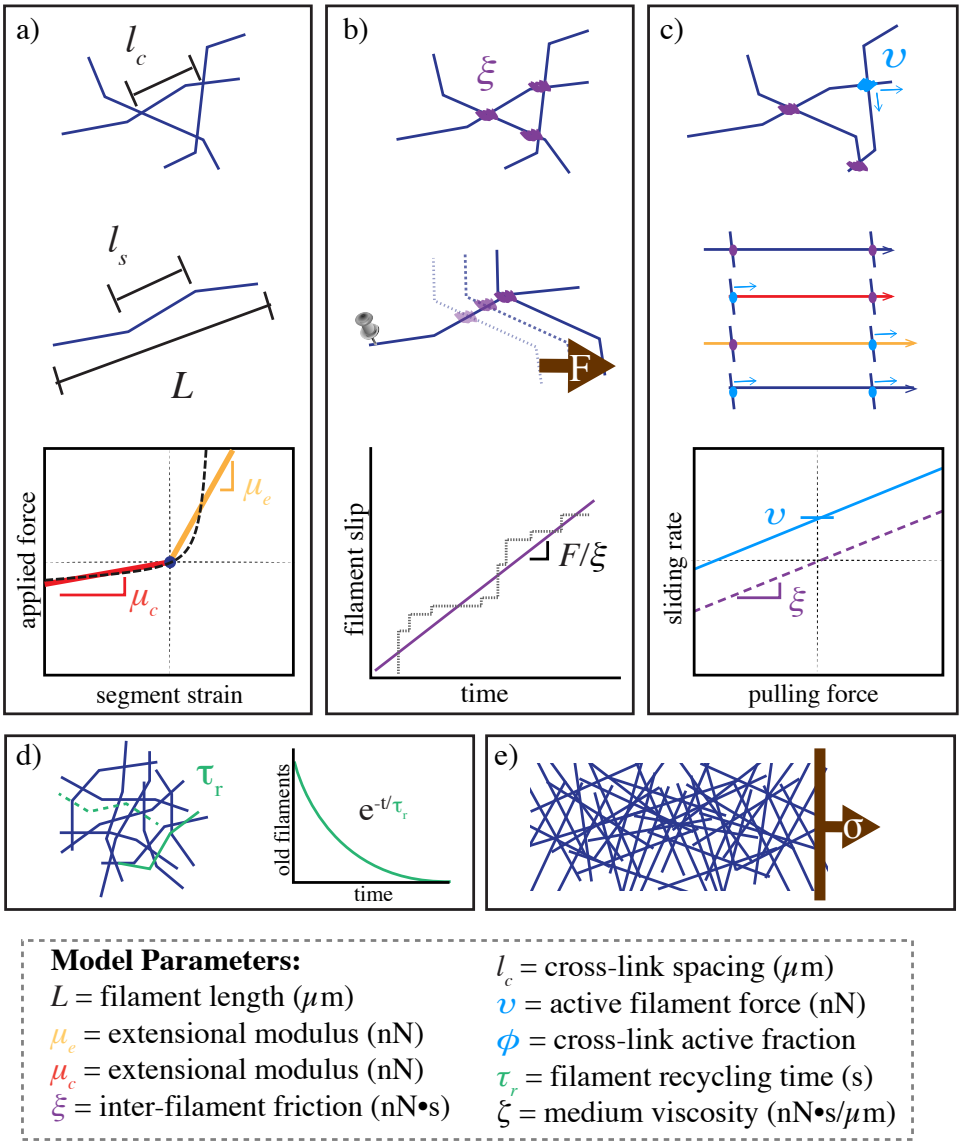

Figure 1. Schematic of modeling framework. a) Filaments are represented as connected chains of spring-like segments with asymmetric compliance.segments have a smaller spring constant for compression than for extension. b) Cross-linking is represented as filament coupling by an effective drag, such that their relative motion is proportional to any applied force. c) Motor activity manifests as a basal sliding rate even in the absence of an external force. d) Only a subset of filament cross-links are active, resulting in differential force exertion along the filament. e) Filaments are turned over at a constant rate, leading to a refreshing in the strain state of all filaments after a characteristic timescale.

Drag-like Coupling Between Overlapping Filaments

Cross-link binding and unbinding is an important element of the overall stress relaxation of a network. In contrast to previous models, we allow relaxation of the network's stored stress by letting the attachment points slip. We do this by replacing an

elastic interaction between pairs of points along filament segments with a drag-like coupling between segments.

$$\mathbf{F_i^\xi} = \xi \cdot \int_{s_{i-1}}^{s_{i+1}} ds \frac{l_s - |s - s_i|}{l_s} \left(\mathbf{v_i} - \mathbf{v_j}\right) p_{ij}(s) \tag{2}$$

Where $p_{ij}(s)$ represents the locational distribution of cross-link points (equal to 1 at locations of cross-links and 0 elsewhere) and $\mathbf{v_i}$ and $\mathbf{v_j}$ represent the the velocities of the ith and jth filament segment. This model assumes a linear relation between applied force and the velocity difference between attached segments. This drag-like coupling has been shown to be an adequate approximation in the case of ionic cross-linking of actin [40, 41], and can be found in the theoretical basis of force-velocity curves for myosin bound filaments [35]. Although non-linearities can arise through force dependent detachment kinetics and/or non-linear force extension of cross-links, we assume that inhomogeneities from non-linear effects are of second or higher order. With this assumption, the motion for the entire network is governed by a dynamical equation of the form

$$L\zeta \mathbf{v_i} + \mathbf{F_i^\xi} = \mathbf{F_i^\mu} \tag{3}$$

Here, the first term in the integral is the filament's intrinsic drag through its embedding fluid, ζ, while the second comes from the drag-like coupling between filaments, ξ.

Active Coupling for Motor Driven Filament Interactions

To add motor activity we select a subset of cross-linked points and impart an additional force of magnitude υ directed in the orientations of the individual filaments, $\mathbf{u_i}$. This leads to a modification of the equation of motion to

$$\mathbf{F_i^\upsilon} = \hat{\mathbf{u}}_\mathbf{i} \cdot \upsilon \int ds \sum_j \frac{l_s - |s - s_i|}{l_s} p_{ij} q_{ij} \tag{4}$$

In this formulation, only at the subset of points where $p_{ij} = 1$ and $q_{ij} = 1$ will there be a force imparted. In our simulations we let q_{ij} be selected randomly such that $\bar{q} = \phi$, where $\bar{q}$ indicates the mean of q.

$$L\zeta \mathbf{v_i} + \mathbf{F_i^\xi} = \mathbf{F_i^\mu} + \mathbf{F_i^\upsilon} \tag{5}$$

2D Network Formation

We follow a mikado model approach by initializing a minimal network of connected unstressed linear filaments in a rectangular 2D domain. We generate 2D networks of these semi-flexible filaments by laying down straight lines of length, L, with random position and orientation. We then assume that some fixed fraction of overlapping filaments become cross-linked (defined in) at their point of overlap.

Although real cytoskeletal networks may form with non-negligible anisotropy, we focus on isotropically initialized networks for simplicity. We define the density using the average distance between cross-links along a filament, l_c. A simple geometrical argument can then be used to derive the number of filaments filling a domain as a function of L and l_c [38]. Here, we use the approximation that the number of filaments needed to tile a rectangular domain of size $W \times H$ is $2WH/Ll_c$, and that the length density is therefore $1/l_c$. In the absence of cross-link slip, we expect the network to form a connected solid with a well defined elastic modulus [38, 39].

System of Equations for Applied Stress

We model our full network as a coupled system of differential equations satisfying 5. Although the general mechanical response of this system may be very complex, we focus our attention on low frequency deformations and the steady-state creep response of the system to an applied stress. To do this we introduce a fixed stress, σ along the midline of our domain. This stress points in the direction, $\hat{\mathbf{x}}$, producing extensional stress.

Finally, we add a 0 velocity constraint at the far edges of our domain of interest. We assume that our network is in the "dry," low Reynold's number limit, where inertial effects are so small that we can equate our total force to 0. Therefore, we have a dynamical system of wormlike chain filaments satisfying

$$L\zeta \mathbf{v_i} + \mathbf{F_i^{\xi}}(\mathbf{v_i}) = \mathbf{F_i^{\mu}}(\mathbf{x_i}) + \mathbf{F_i^{v}}(\mathbf{x_i}) + \sigma \hat{\mathbf{u}}(\mathbf{x_i}) \tag{6}$$

subject to constraints such that $\mathbf{v_i}(\mathbf{x})$ is 0 with $x = 0$. This results in an implicit differential equation for filament segments which can be discretized and integrated in time to produce a solution for the motion of the system.

Filament Recycling as a model for rapid filament turnover

To simplify the complex biochemical changes that can give rise to actin filament polymerization and depolymerization, we chose to use simple filament appearance and disappearance as a lowest order model of filament recycling. In this sense the average lifetime of a filament between it's appearance and disappearance would be τ_r. In order to do this without causing an unnecessary bias in the results, at a regularized interval $\tau_s < 0.01 \cdot \tau_r$, we selected τ_s/τ_r filaments, reset their extension or compression to 0, and relocated them to a random position and orientation. This has the effect of creating an approximately exponential decay in the number of old filaments over time.

Computational Simulation Method

We tested our analytical conclusions on a computational model. More technical details of the model can be found in the Appendix, but we summarize the main modeling points here.

We discretize the filaments such that the equations of motion becomes a coupled system of equations for the velocities of filament endpoints, $\mathbf{x}$. The drag-like force between overlapping filaments results in a coupling of the velocities of endpoints.

$$\mathbf{A} \cdot \dot{\mathbf{x}} = \mathbf{f}(\mathbf{x}) \tag{7}$$

where $\mathbf{A}$ represents a coupling matrix between endpoints of filaments that overlap, and $\mathbf{f}(\mathbf{x})$ is the spring force between pairs of filament segment endpoints. We can then numerically integrate this system of equations to find the time evolution of the positions of all filament endpoints.

We generate a network by laying down filaments with random position and orientation within a domain of size D_x by D_y with periodic boundaries in the y-dimension. The external stress (shear or extensional/compressional) is applied to all filament endpoints falling within a fixed x-distance from the center of the domain. Finally, filament endpoints falling within a fixed x-distance from the edges of the domain are constrained to be nonmoving. All filament interactions, force fields, and constraints are smoothed over small regions such that the equations will contain no sharp discontinuities.

The nominal units for length, force, and time are μm, nN, and s, respectively. We explored parameter space around an estimate of biologically relevant parameter values, given in Table 1.

Table 1. Simulation Parameter Values

parameter	symbol	physiological estimate
extensional modulus	μ_e	$10nN$
compressional modulus	μ_c	$0.1nN$
cross-link drag coefficient	ξ	$unknown$
medium drag coefficient	ζ	$0.0005\frac{nNs}{\mu m^2}$
filament length	L	$5\mu m$
cross-link spacing	l_c	$0.5\mu m$
domain size	$D_x \times D_y$	$20 \times 50\mu m$

Results and Discussion

We used our model to tease apart the complex interdependence of passive and active network properties on the patterning and rates of cortical flow. To begin, we addressed the effect of filament recycling on the deformation of a network without motor activity in the presence of a constant external force. After we had established the timescales of passive deformation, we approached the active case and made similar measurements of the timescales of internal stress buildup and dissipation. Finally, we were able to synthesize our understanding of the passive and active systems to analyze the behavior of a more complex situation of an actively flowing network.

Filament recycling prevents cortical tearing and modulates the viscous stress relaxation of passive filament networks

Networks with passive cross-links and no filament turnover undergo three stages of deformation in response to an extensional force. We first probed the network's passive response by imposing an external force on our simulated network in the absence of recycling. As shown in Figure 2.a, by applying a force at the boundary of a patch of network, we induced a rightward deformation of the network. The deformation occurred in three phases corresponding to the three example networks in Figure 2.a. On short timescales the networked quickly responded by elastically approaching a fixed strain γ_0, similar to that predicted by [38]. On longer timescales, we found that the network continued deforming more slowly as filaments were able to slip past each other. Finally, as the network continued to dilate viscously, the connectivity of the network decreased. Eventually connected patches became isolated and the network teared, resulting in the highly heterogeneous network structure shown in the t=440 example of Figure 2.a.

We next analyzed the force and velocity data of the network at individual time points to determine what kind of deformation the material was undergoing. As shown by the data in Figure 2.b corresponding to the simulation at time t=88s, during this stage, the stress profile (blue) is nearly constant throughout the material while the velocity profile (orange) is linear in space. These are two indications that a purely viscous description is adequate for this stage of deformation. By measuring the mean material stress and strain rate ($\overline{v_i/x_i}$) at every time point, we generated a measurement of the material strain through time as shown in Figure 2.c. From this figure, we can see the three phases of deformation outlined in Figure 2.a. It's clear that there are two phases in the stress and strain profile: one characterized by a rapid buildup of internal stress and strain, and one where the internal stress remains constant and the strain increases more slowly. We define the transition time between this fast, elastic response and the slower, viscous response as τ_c. For times longer than τ_c the material underwent a steady continuous straining at a nearly constant rate. This linear relationship between strain and time characterizes a material with an effective viscosity, η, given by the ratio

of the applied stress to the strain rate (i.e $\sigma/\dot{\gamma}$). At very long times, this constant strain rate behavior begins to break down. As the network strains beyond 10% or so, network connectivity decreases, and the strain rate of the network begins to increase. This strain thinning behavior can be seen in the hockey-stick shape of the inset of Figure 2.c.

DISCUSS

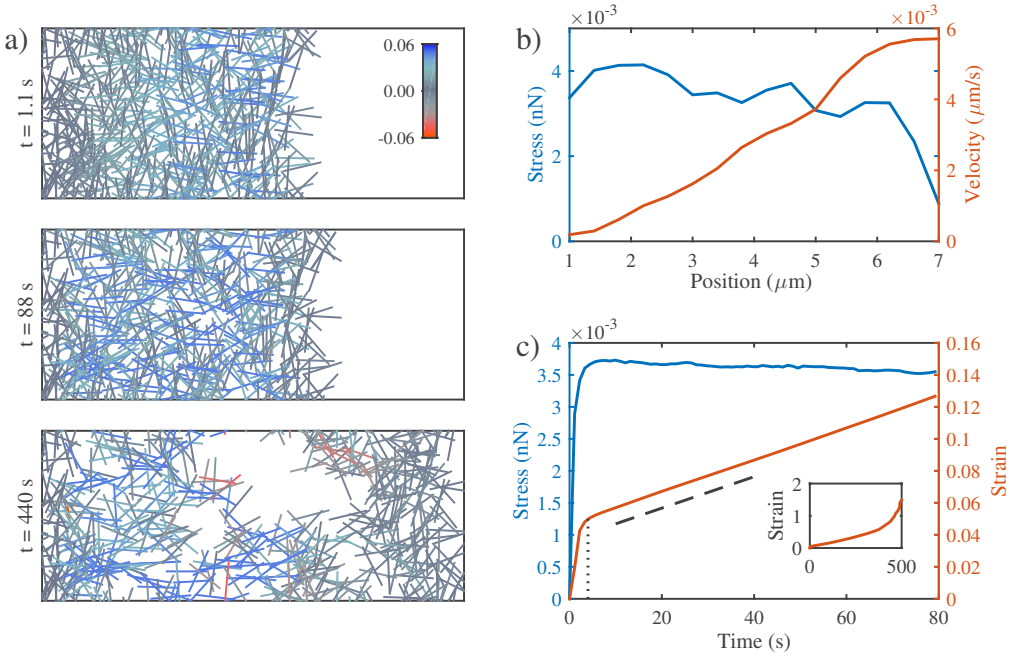

Figure 2. Networks with passive cross-links and no filament turnover undergo three stages of deformation in response to an extensional force. **a)** Three successive time points from a simulation of a $4 \times 10\,\mu m$ network deforming under an applied extensional stress of $0.005\ nN/\mu m$. In this and all subsequent figures, filaments are color-coded with respect state of stress (blue = tension, red = compression). Network parameters: $L = 1\,\mu m$, $l_c = 0.3\,\mu m$, $\xi = 100\,nN \cdot s$. **b)** Mean filament stress and velocity profiles for the network in (a) at t=88s. Note that the stress is nearly constant and the velocity is nearly linear as predicted for a viscous fluid under extension. **c)** Plots of the mean stress and strain vs time for the simulation in (a), illustrating the three stages of deformation: (i) A fast initial phase accompanies rapid buildup of internal network stress; (ii) after a characteristic time τ_c s (indicated by vertical dotted line) the network deforms like a material with a constant effective viscosity, η_c, as indicated by the slope of the dashed line. (inset) At long times, the strain accelerates as the network undergoes strain thinning and eventually tears.

Network architecture sets the rate and timescales of deformation. To better understand the origins of the timescale of viscous behavior and the effective viscosity, we measured these features for a variety of network setups and applied stresses. Across a wide swath of parameter space, the network is always capable of reaching a point of viscous deformation with an effective viscosity. By measuring the rate of deformation during the phase of constant strain rate, we could measure the effective viscosity and determining which network parameters were responsible for setting the value. From our observations, we were able to determine that the effective viscosity of a network was proportional to the friction coefficient of the individual cross-links, ξ, as well as the square of the number of cross-links on a given filament

$(L/l_c - 1)^2$. A simple theoretical derivation (See Supp.) allowed us to estimate a numerical constant of proportionality of $\pi/4$. As shown in Figure 3.a, the theoretical prediction agrees very well with the measured values form the simulation.

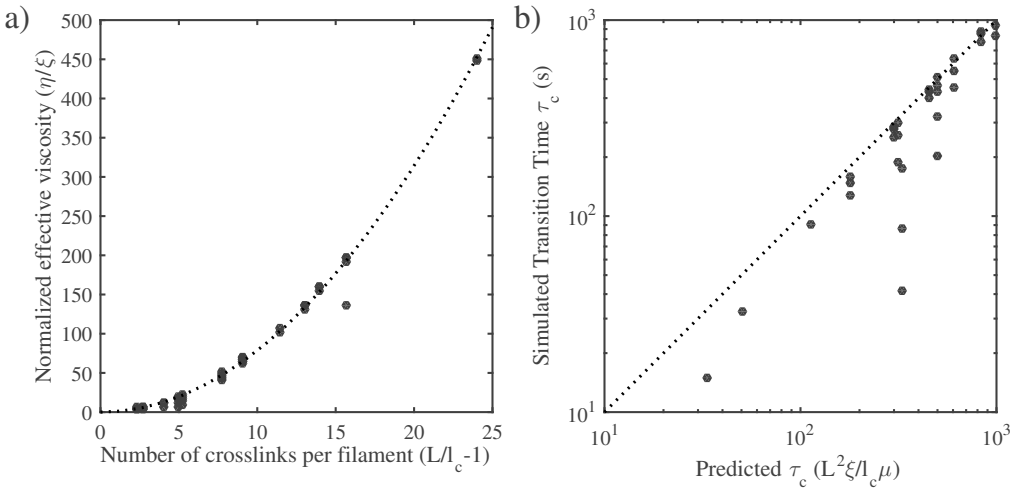

Figure 3. Network architecture sets the rate and timescales of deformation. **a)** The effective viscosity depends on the drag coefficient and the density of the network. Data points are the normalized effective viscosity from simulations (effective viscosity measured in fluid phase divided by the cross link friction coefficient) vs the number of cross links per filament (L/lc - 1). Dotted line indicates the relationship predicted by a simple theory, $\eta_c = \xi(L/l_c - 1)^2$ **b)** The transition to viscous behavior occurs at a characteristic time, τ_c, that is set by the ratio of the elastic modulus predicted in [38] (i.e. $G_0 \approx \mu/l_c$) to the effective viscosity, η_c.

We were also interested in determining what sets the timescale of the transition from elastic to viscous behavior. In many simple viscoelastic materials, the ratio of the elastic modulus, G_0, to the viscosity, η_c is a general indicator of the transition timescale from elastic to viscous behavior. Using the approximation of the equation for elastic modulus from [38], $G_0 \approx \mu/l_c$, we predict a crossover time, $\tau_c \approx L^2\xi/l_c\mu$. By measuring the time at which the strain rate of the became nearly constant we were able to determine an estimate of this time for a wide variety of simulation parameters as well. Indeed, as shown in Figure 3.b, our approximation is in good agreement with the observed transition time. This served as a good indication that our model was consistent with known models for viscoelastic semi flexible polymer networks.

Filament recycling rescues network tearing and modulates effective viscosity.

Filament recycling allows persistent stress buildup in active networks

Next we tackled the case of a network with spatially isotropic motor activity. We found that our simulation axioms were able to produce transient contraction of a patch of free-floating network. As shown in Figure **??** a, the contraction extent was strongly dependent on the magnitudes of both the filament asymmetry and the motor activity scale. Additionally, contraction would only occur when there was fractional motor activity, $\phi < 1$, (see supplement). The contraction was able to take place over a time

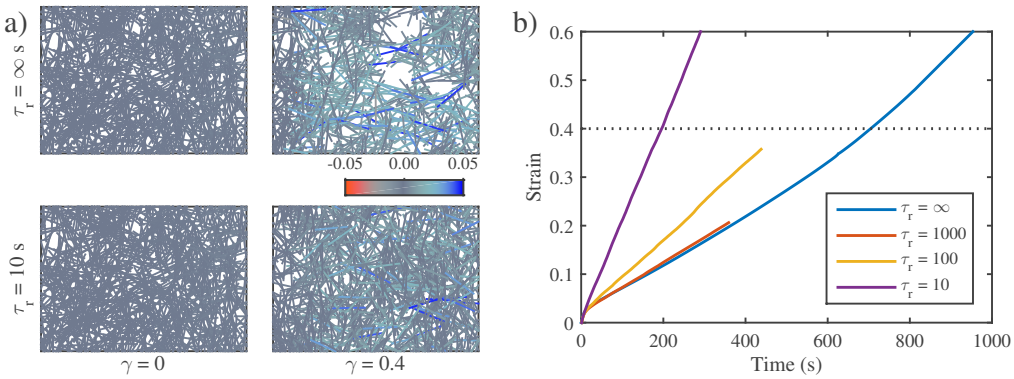

Figure 4. Filament recycling rescues network tearing and modulates effective viscosity. **a)** Examples of $20 \times 12 \mu m$ network under 0.001 $nN/\mu m$ extensional stress with recycling ($\tau_r = 10s$) and without, ($\tau_r = \infty$). Both images are taken when the patches had reached a net strain of 0.4. The network with recycling doesn't appear to change shape because its components have been recycled to remain in the original domain. Network parameters: $L = 3\,\mu m$, $l_c = 0.5\,\mu m$, $\xi = 10\,nN \cdot s$. **b)** Strain buildup for networks with parameters as in a) in the presence of different filament recycling rates. Dotted line indicates the strain state at which the snapshots in panel a) were taken. Note that the strain rate for $\tau_r = 1000$ is essentially identical to that of $\tau_r = \infty$, indicating that recycling does not govern the relaxation rate if the recycling time is above a threshold.

scale, τ_c, but on time scales much longer the contraction would stall and polarity sorting would begin to dominate.

Due to the long term polarity sorting and the fact that filament recycling would be difficult to incorporate into a moving material, we additionally analyzed the stress buildup in a patch that was constrained to maintain its original area. As shown in Figure **??** b, the results showed a period of net stress due to an imbalance between larger stresses from extended filaments and smaller stresses from compressed filaments. After a characteristic timescale τ_a, the extensional stress peaks and begins to decrease while the compressive stresses continue to build up resulting in the extensional and compressive stresses beginning to cancel each other. After another time period, τ_{eq}, the internal stresses become balanced and the net stress drops to approximately 0. The timescale and magnitude of the peak stresses agree with a qualitative expectation discussed later.

Upon the addition of filament recycling, we were able to find that the network maintained a nonzero net stress for times much longer than $\tau_e q$. We refer to this as the steady state stress because based on our simulations it doesn't appear that this stress ever subsides, and duh. For similar network parameters as illustrated in Figure **??** c iii, we found that the steady state stress was well predicted by the comparison between the timescale of recycling, τ_r and that of peak activity, τ_a.

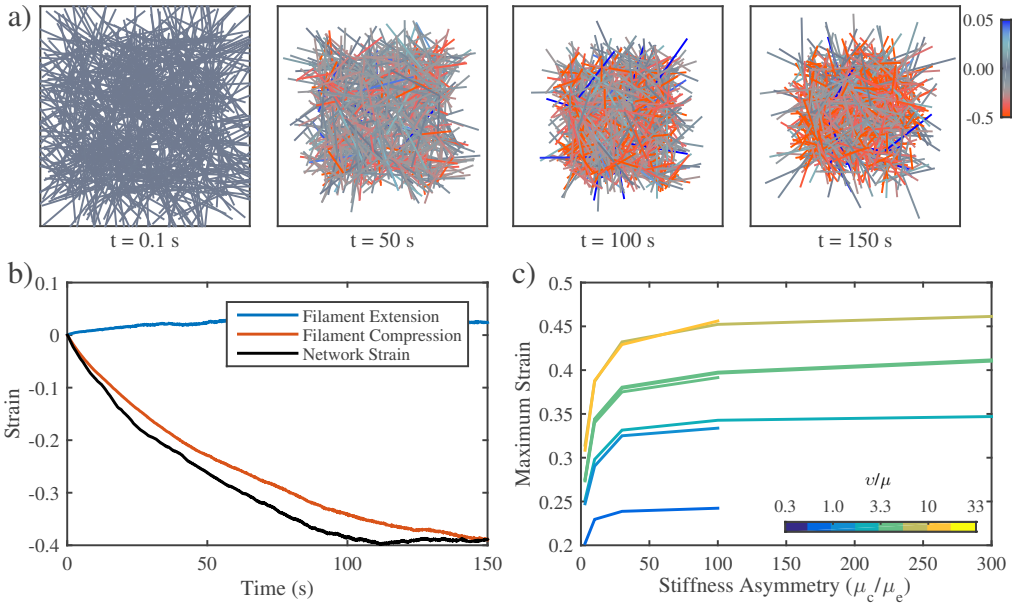

Figure 5. In the absence of filament recycling, active networks with free boundaries contract and then stall against passive resistance to network compression. **a)** Example of an active network contracting. Note the buildup of compressive stress as contraction approaches stall between 100 s and 150 s. Network parameters: $L = 5\,\mu m$, $l_c = 0.3\,\mu m$, $\xi = 100\,nN \cdot s$, $v = 0.1\,nN$. **b)** Plots showing time evolution of total network strain and the average extensional (blue) or compressive (red) strain on individual filaments. **c)** The network's ability to deform requires asymmetric filament compliance. Total network strain also increases with the applied myosin force v.

Filament recycling modulates the balance between active stress buildup and viscous stress relaxation to set the flow rate in polarized networks

Supporting Information

Acknowledgments

We would like to thank Shiladitya Banerjee and Patrick McCall for stimulating discussions.

References

1. Bray D, White J. Cortical flow in animal cells. Science. 1988;239(4842):883–888. Available from: http://www.sciencemag.org/content/239/4842/883.abstract.

2. Hird SN, White JG. Cortical and cytoplasmic flow polarity in early embryonic cells of Caenorhabditis elegans. The Journal of Cell Biology. 1993;121(6):1343–1355. Available from: http://jcb.rupress.org/content/121/6/1343.abstract.

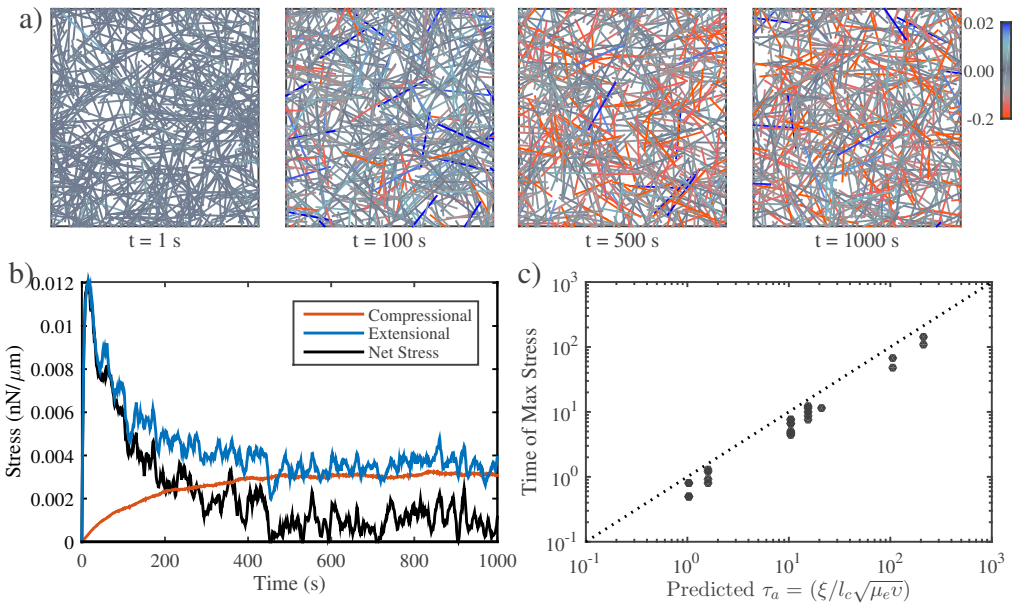

Figure 6. In the absence of filament recycling, active networks can only exert a transient force against a fixed boundary. **a)** Simulation of an active network with fixed boundaries illustrating progressive buildup of internal stress through local filament rearrangement and deformation. Note the progressive buildup of compressive stress on individual filaments. Network parameters: $L = 5\,\mu m$, $l_c = 0.3\,\mu m$, $\xi = 100\,nN \cdot s$, $\upsilon = 0.1\,nN$. **b)** Plots of total network stress and the average extensional (blue) and compressive (red) stress on individual filaments for the simulation shown in (a). Rapid buildup of extensional stress allows the network transiently to exert force on its boundary, but this force is dissipated at longer times as as internal extensional and compressive stresses become balanced. **c**. Measurement and prediction of the characteristic time (τ_a) at which the maximum stress is achieved.

3. Munro E, Nance J, Priess JR. Cortical Flows Powered by Asymmetrical Contraction Transport {PAR} Proteins to Establish and Maintain Anterior-Posterior Polarity in the Early C. elegans Embryo. Developmental Cell. 2004;7(3):413 – 424. Available from: http://www.sciencedirect.com/science/article/pii/S153458070400276X.

4. Mayer M, Depken M, Bois JS, Julicher F, Grill SW. Anisotropies in cortical tension reveal the physical basis of polarizing cortical flows. Nature. 2010 09;467(7315):617–621. Available from: http://dx.doi.org/10.1038/nature09376.

5. Bois JS, Jülicher F, Grill SW. Pattern Formation in Active Fluids. Phys Rev Lett. 2011 Jan;106:028103. Available from: http://link.aps.org/doi/10.1103/PhysRevLett.106.028103.

6. Salbreux G, Prost J, Joanny JF. Hydrodynamics of Cellular Cortical Flows and the Formation of Contractile Rings. Phys Rev Lett. 2009 Jul;103:058102. Available from: http://link.aps.org/doi/10.1103/PhysRevLett.103.058102.

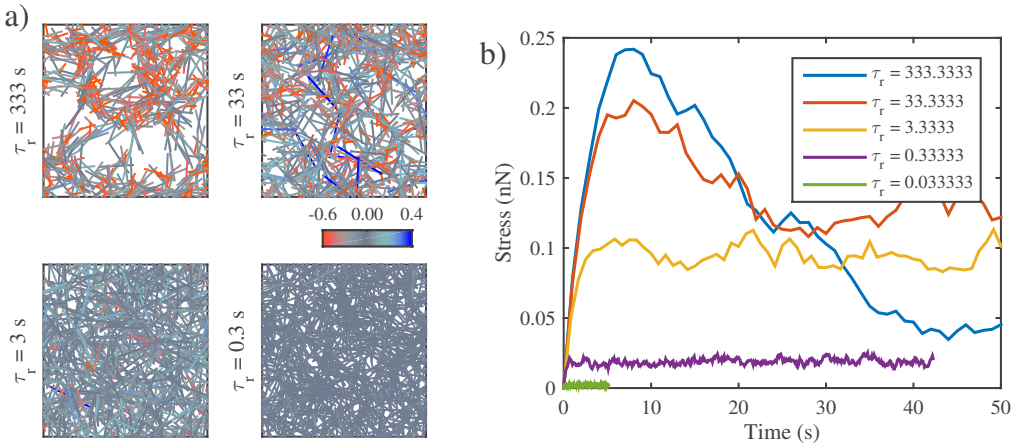

Figure 7. Filament recycling allows network to exert sustained stress on a fixed boundary. **a)** Example simulations of active networks and fixed boundaries for different timescales of filament recycling. Network parameters are the same as in Figure 6, except that the active force (v = 1) has been increased to emphasize the effects of internal network remodeling under stress. Note that significant remodeling occurs for longer recycling times. **b)** Plots of net stress for different recycling times; for long-lived filaments, stress is built rapidly, but then dissipates. Increasing filament turnover rates reduces stress dissipation by recycling compressed filaments; however, very short recycling times prevent any stress from being built up in the first place.

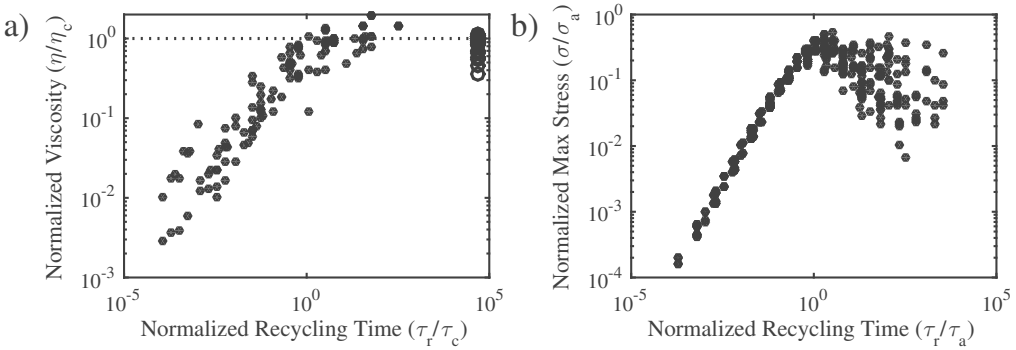

Figure 8. Filament recycling tunes the magnitude of effective viscosity and steady state stress. **a)** Normalized effective viscosities as a function of the normalized recycling time. When the recycling timescale is significantly less than the passive relaxation timescale (see Figure 3), the viscosity of the network becomes dependent on recycling time. **b)** Normalized steady state stress as a function of normalized recycling time. The steady state stress is set by the timescale at which the network strain is refreshed relative to the timescale at which the max stress is reached.

7. Hochmuth RM. Micropipette aspiration of living cells. Journal of Biomechanics. 2000;33(1):15 – 22. Available from: `http://www.sciencedirect.com/science/article/pii/S002192909900175X`.

8. Evans E, Yeung A. Apparent viscosity and cortical tension of blood granulocytes determined by micropipet aspiration. Biophysical Journal. 1989 07;56(1):151–160. Available from: `http://www.ncbi.nlm.nih.gov/pmc/articles/PMC1280460/`.

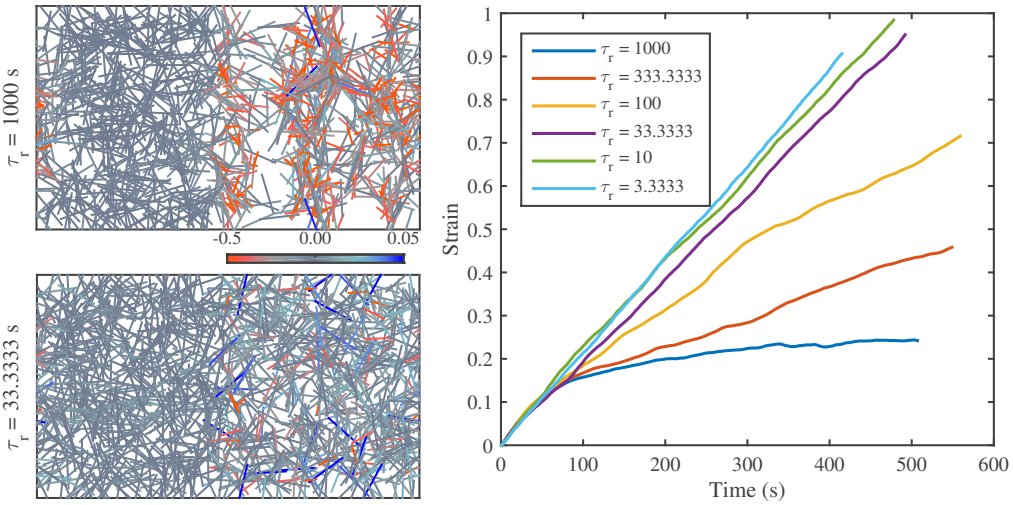

Figure 9. Filament recycling allows sustained flows in networks with non-isotropic activity. **a)** Example simulations of non-isotropic networks with long ($\tau_r = 1000$) and short ($\tau_r = 33$) recycling timescales. In these networks the left half of the network is passive while the right half is active. Network parameters: $L = 5\,\mu m$, $l_c = 0.3\,\mu m$, $\xi = 100\,nN \cdot s$, $\upsilon = 1\,nN$. **b)** Graph of strain for identical networks varying recycling timescales. With long recycling times, the network stalls; reducing the recycling timescale allows the network to persist in its deformation. However, for the shortest recycling timescales, the steady state strain appears to approach an asymptotic limit.

9. Bausch AR, Ziemann F, Boulbitch AA, Jacobson K, Sackmann E. Local Measurements of Viscoelastic Parameters of Adherent Cell Surfaces by Magnetic Bead Microrheometry. Biophysical Journal. 1998;75(4):2038 – 2049. Available from: http://www.sciencedirect.com/science/article/pii/S0006349598776465.

10. Wachsstock DH, Schwarz WH, Pollard TD. Cross-linker dynamics determine the mechanical properties of actin gels. Biophysical Journal. 1994;66(3, Part 1):801 – 809. Available from: http://www.sciencedirect.com/science/article/pii/S0006349594808562.

11. Lieleg O, Claessens MMAE, Luan Y, Bausch AR. Transient Binding and Dissipation in Cross-Linked Actin Networks. Phys Rev Lett. 2008 Sep;101:108101. Available from: http://link.aps.org/doi/10.1103/PhysRevLett.101.108101.

12. Lieleg O, Schmoller KM, Claessens MMAE, Bausch AR. Cytoskeletal Polymer Networks: Viscoelastic Properties are Determined by the Microscopic Interaction Potential of Cross-links. Biophysical Journal. 2009 6;96(11):4725–4732. Available from: http://www.sciencedirect.com/science/article/pii/S0006349509007589.

13. Yao NY, Becker DJ, Broedersz CP, Depken M, MacKintosh FC, Pollak MR, et al. Nonlinear Viscoelasticity of Actin Transiently Cross-linked with Mutant alpha-Actinin-4. Journal of Molecular Biology. 2011;411(5):1062 – 1071. Available from: http://www.sciencedirect.com/science/article/pii/S0022283611007376.

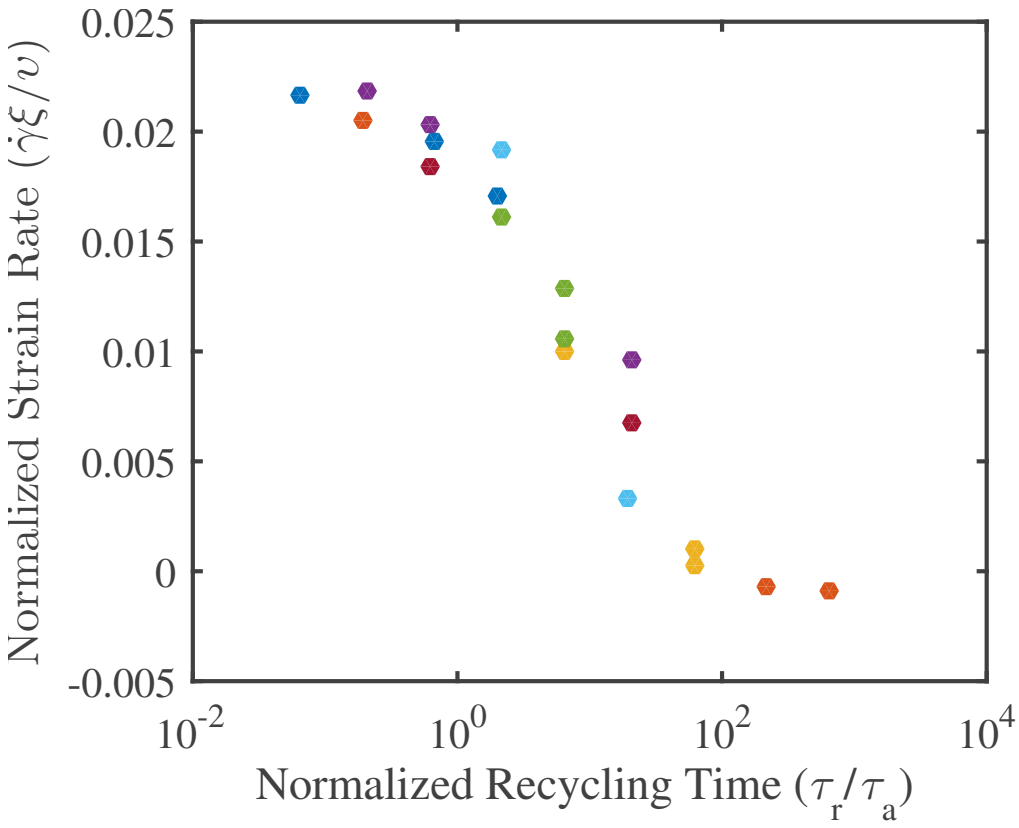

Figure 10

14. Liu J, Koenderink GH, Kasza KE, MacKintosh FC, Weitz DA. Visualizing the Strain Field in Semiflexible Polymer Networks: Strain Fluctuations and Nonlinear Rheology of *F*-Actin Gels. Phys Rev Lett. 2007 May;98:198304. Available from: `http://link.aps.org/doi/10.1103/PhysRevLett.98.198304`.

15. Broedersz CP, Depken M, Yao NY, Pollak MR, Weitz DA, MacKintosh FC. Cross-Link-Governed Dynamics of Biopolymer Networks. Phys Rev Lett. 2010 Nov;105:238101. Available from: `http://link.aps.org/doi/10.1103/PhysRevLett.105.238101`.

16. Müller KW, Bruinsma RF, Lieleg O, Bausch AR, Wall WA, Levine AJ. Rheology of Semiflexible Bundle Networks with Transient Linkers. Phys Rev Lett. 2014 Jun;112:238102. Available from: `http://link.aps.org/doi/10.1103/PhysRevLett.112.238102`.

17. Kim T, Hwang W, Kamm RD. Dynamic Role of Cross-Linking Proteins in Actin Rheology. Biophysical Journal. 2011 10;101(7):1597–1603. Available from: `http://www.ncbi.nlm.nih.gov/pmc/articles/PMC3183755/`.

18. Lieleg O, Bausch AR. Cross-Linker Unbinding and Self-Similarity in Bundled Cytoskeletal Networks. Phys Rev Lett. 2007 Oct;99:158105. Available from: `http://link.aps.org/doi/10.1103/PhysRevLett.99.158105`.

19. Kim T, Gardel ML, Munro E. Determinants of Fluidlike Behavior and Effective Viscosity in Cross-Linked Actin Networks. Biophysical Journal. 2014;106(3):526 –

534. Available from:
http://www.sciencedirect.com/science/article/pii/S0006349513058487.

20. Murrell MP, Gardel ML. F-actin buckling coordinates contractility and severing in a biomimetic actomyosin cortex. Proceedings of the National Academy of Sciences. 2012;109(51):20820–20825. Available from:
http://www.pnas.org/content/109/51/20820.abstract.

21. Lenz M, Gardel ML, Dinner AR. Requirements for contractility in disordered cytoskeletal bundles. New Journal of Physics. 2012;14(3):033037. Available from:
http://stacks.iop.org/1367-2630/14/i=3/a=033037.

22. Lenz M. Geometrical Origins of Contractility in Disordered Actomyosin Networks. Phys Rev X. 2014 Oct;4:041002. Available from:
http://link.aps.org/doi/10.1103/PhysRevX.4.041002.

23. Köhler S, Bausch AR. Contraction Mechanisms in Composite Active Actin Networks. PLoS ONE. 2012 07;7(7):e39869. Available from:
http://dx.doi.org/10.1371%2Fjournal.pone.0039869.

24. Alvarado J, Sheinman M, Sharma A, MacKintosh FC, Koenderink GH. Molecular motors robustly drive active gels to a critically connected state. Nat Phys. 2013 09;9(9):591–597. Available from: http://dx.doi.org/10.1038/nphys2715.

25. Banerjee S, Marchetti MC. Instabilities and oscillations in isotropic active gels. Soft Matter. 2011;7:463–473. Available from:
http://dx.doi.org/10.1039/C0SM00494D.

26. Liverpool TB, Marchetti MC, Joanny JF, Prost J. Mechanical response of active gels. EPL (Europhysics Letters). 2009;85(1):18007. Available from:
http://stacks.iop.org/0295-5075/85/i=1/a=18007.

27. Koenderink GH, Dogic Z, Nakamura F, Bendix PM, MacKintosh FC, Hartwig JH, et al. An active biopolymer network controlled by molecular motors. Proceedings of the National Academy of Sciences of the United States of America. 2009 09;106(36):15192–15197. Available from:
http://www.ncbi.nlm.nih.gov/pmc/articles/PMC2741227/.

28. Zumdieck A, Kruse K, Bringmann H, Hyman AA, Jülicher F. Stress Generation and Filament Turnover during Actin Ring Constriction. PLoS ONE. 2007 08;2(8):e696. Available from:
http://dx.plos.org/10.1371/journal.pone.0000696.

29. Hiraiwa T, Salbreux G. Role of turn-over in active stress generation in a filament network. ArXiv e-prints. 2015 Jul;.

30. Mak M, Zaman MH, Kamm RD, Kim T. Interplay of active processes modulates tension and drives phase transition in self-renewing, motor-driven cytoskeletal networks. Nat Commun. 2016 01;7. Available from:
http://dx.doi.org/10.1038/ncomms10323.

31. Dierkes K, Sumi A, Solon J, Salbreux G. Spontaneous Oscillations of Elastic Contractile Materials with Turnover. Phys Rev Lett. 2014 Oct;113:148102. Available from:
http://link.aps.org/doi/10.1103/PhysRevLett.113.148102.

32. Vanossi A, Manini N, Urbakh M, Zapperi S, Tosatti E. *Colloquium* : Modeling friction: From nanoscale to mesoscale. Rev Mod Phys. 2013 Apr;85:529–552. Available from: http://link.aps.org/doi/10.1103/RevModPhys.85.529.

33. Spruijt E, Sprakel J, Lemmers M, Stuart MAC, van der Gucht J. Relaxation Dynamics at Different Time Scales in Electrostatic Complexes: Time-Salt Superposition. Phys Rev Lett. 2010 Nov;105:208301. Available from: http://link.aps.org/doi/10.1103/PhysRevLett.105.208301.

34. Filippov AE, Klafter J, Urbakh M. Friction through Dynamical Formation and Rupture of Molecular Bonds. Phys Rev Lett. 2004 Mar;92:135503. Available from: http://link.aps.org/doi/10.1103/PhysRevLett.92.135503.

35. Banerjee S, Marchetti MC, Müller-Nedebock K. Motor-driven dynamics of cytoskeletal filaments in motility assays. Phys Rev E. 2011 Jul;84:011914. Available from: http://link.aps.org/doi/10.1103/PhysRevE.84.011914.

36. Sanchez T, Chen DTN, DeCamp SJ, Heymann M, Dogic Z. Spontaneous motion in hierarchically assembled active matter. Nature. 2012 11;491(7424):431–434. Available from: http://dx.doi.org/10.1038/nature11591.

37. Broedersz CP, Storm C, MacKintosh FC. Effective-medium approach for stiff polymer networks with flexible cross-links. Phys Rev E. 2009 Jun;79:061914. Available from: http://link.aps.org/doi/10.1103/PhysRevE.79.061914.

38. Head DA, Levine AJ, MacKintosh FC. Deformation of Cross-Linked Semiflexible Polymer Networks. Phys Rev Lett. 2003 Sep;91:108102. Available from: http://link.aps.org/doi/10.1103/PhysRevLett.91.108102.

39. Wilhelm J, Frey E. Elasticity of Stiff Polymer Networks. Phys Rev Lett. 2003 Sep;91:108103. Available from: http://link.aps.org/doi/10.1103/PhysRevLett.91.108103.

40. Ward A, Hilitski F, Schwenger W, Welch D, Lau AWC, Vitelli V, et al. Solid friction between soft filaments. Nat Mater. 2015 03;advance online publication:–. Available from: http://dx.doi.org/10.1038/nmat4222.

41. Chandran PL, Mofrad MRK. Averaged implicit hydrodynamic model of semiflexible filaments. Phys Rev E. 2010 Mar;81:031920. Available from: http://link.aps.org/doi/10.1103/PhysRevE.81.031920.